IEEE Access
Multidisciplinary | Rapid Review | Open Access Journal

Received November 20, 2020, accepted December 6, 2020, date of publication December 18, 2020,
date of current version December 31, 2020.

*Digital Object Identifier 10.1109/ACCESS.2020.3045732*

# An Integrated Design for Classification and Localization of Diabetic Foot Ulcer Based on CNN and YOLOv2-DFU Models

**JAVARIA AMIN[1], MUHAMMAD SHARIF[2], (Senior Member, IEEE), MUHAMMAD ALMAS ANJUM[3], HABIB ULLAH KHAN[4], (Member, IEEE), MUHAMMAD SHERAZ ARSHAD MALIK[5], AND SEIFEDINE KADRY[6], (Senior Member, IEEE)**

[1]Department of Computer Science, University of Wah, Wah Cantonment 47040, Pakistan
[2]Department of Computer Science, Comsats University Islamabad–Wah, Wah Cantonment 45550, Pakistan
[3]College of Electrical & Mechanical Engineering, National University of Sciences & Technology (NUST), Islamabad 24090, Pakistan
[4]Department of Accounting & Information Systems, College of Business and Economics, Qatar University, Doha, Qatar
[5]Department of Information Technology, Government College University Faisalabad, Faisalabad 38000, Pakistan
[6]Department of Mathematics and Computer Science, Faculty of Science, Beirut Arab University, Beirut 1107 2809, Lebanon

Corresponding authors: Muhammad Sharif (muhammadsharifmalik@yahoo.com) and Habib Ullah Khan (habib.khan@qu.edu.qa)

This work was supported by the Qatar National Library, Doha, Qatar.

**ABSTRACT** Diabetes is a chronic disease, if not treated in time may lead to many complications including diabetic foot ulcers (DFU). DFU is a dangerous disease, it needs regular treatment otherwise it may lead towards foot amputation. The DFU is classified into two categories such as infection (bacteria) and the ischaemia (inadequate supply of the blood). The DFU detection at an initial phase is a tough procedure. Therefore in this research work 16 layers convolutional neural network (CNN) for example 01 input, 03 convolutional, 03 batch-normalization, 01 average pooling, 01 skips convolutional, 03 ReLU, 01 add (element-wise addition of two inputs), fully connected, softmax and classification output layers for classification and YOLOv2-DFU for localization of infection/ischaemia models are proposed. In the classification phase, deep features are extracted and supplied to the number of classifiers such as KNN, DT, Ensemble, softmax, and NB to analyze the classification results for the selection of best classifiers. After the experimentation, we observed that DT and softmax achieved consistent results for the detection of ischaemia/infection in all performance metrics such as sensitivity, specificity, and accuracy as compared with other classifiers. In addition, after the classification, the Gradient-weighted class activation mapping (Grad-Cam) model is used to visualize the high-level features of the infected region for better understanding. The classified images are passed to the YOLOv2-DFU network for infected region localization. The Shuffle network is utilized as a mainstay of the YOLOv2 model in which bottleneck extracted features through ReLU node-199 layer and passed to the YOLOv2 model. The proposed method is validated on the newly developed DFU-Part (B) dataset and the results are compared with the latest published work using the same dataset.

**INDEX TERMS** YOLOv2-DFU, convolutional, batch-normalization, and shuffle net, ReLU.

## I. INTRODUCTION

Diabetic foot ulcer (DFU) is caused owing to complications of diabetes that may lead to the elimination of limb or the foot [1]. DFU is located commonly on the bottom side of the foot. The major symptoms of the DFU are skin color changes, variation in the temperature of the skin, foot swelling, legs pains, and dry cracks. Globally, DFU treatment takes high cost and if not treated at an early stage then the mortality rate is increased. Ischaemia/infection region classification and recognition are the most vital parameters to predict DFU healing chances or amputation risk [2]. In the human body, ischaemia is caused due to deficiency of blood circulation, and the same is developed owing to the chronic obstacles of diabetes [3]. It is detected through palpating pulses in the foot [4] and visually ischaemia appearance can be shown through the presence of the poor foot reperfusion which may lead towards the infection of DFU [5]. The DFU detection

The associate editor coordinating the review of this manuscript and approving it for publication was Yudong Zhang.

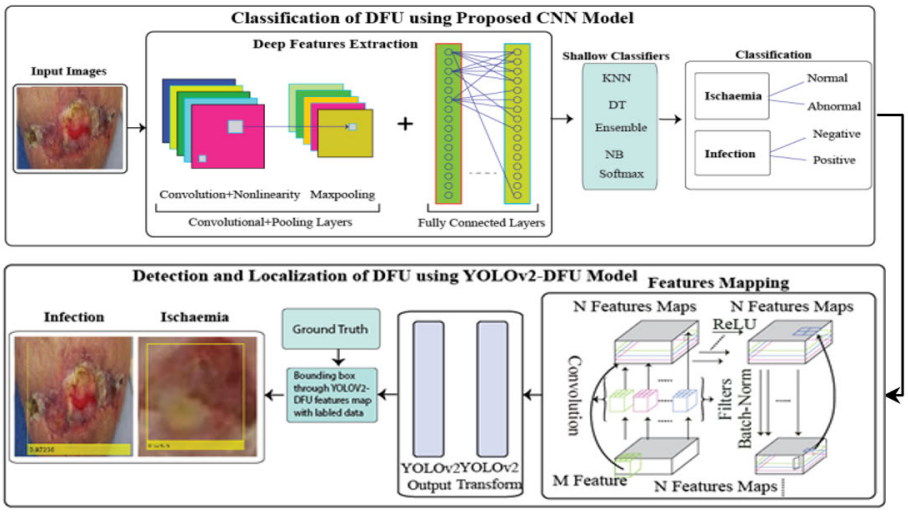


**FIGURE 1.** Overview of the proposed architecture (proposed method classifies and localize the different types of DFU such as Ischaemia (normal and ischaemia images) and infection (normal and infection images).

is a challenging task for the researchers because of (i) lighting condition (ii) high similarity in inter and the intraclass variations (iii) foot ulcer appears in variable size, shape, and location. Accurate diagnosis of DFU requires complete medical history including physical examination the bacteriological study, blood tests, and in-depth study related to leg blood vessels. Mostly these resources and the tests are not available around the world.

To overcome these limitations computerized methods are required to classify/ localize the DFU at an early stage [6]. By considering the existing literature, in this research deep learning approaches are investigated for classification and localization of the DFU. In this work new deep learning models are designed after the comprehensive experiments. In addition, proposed models are trained from scratch using diabetic foot images.

The major contributions of the proposed method are:

- The CNN model having sixteen layers is proposed to classify the DFU into ischaemia/infection.
- The YOLOv2-DFU model is developed, in which ShuffleNet is used as a backbone of the YOLOv2 architecture for localization of the DFU to the corresponding class labels as well as confidence scores.

The organization of the paper is as: Associated work is discussed in Section II, the projected technique is discussed in Section III and the experiment/results are presented in Section IV. Paper is concluded with future research directions in Section V and Section VI correspondingly.

## II. RELATED WORK

The existing DFU methods are discussed in detail [7]–[13]. The edge detection, morphological operations, and unsupervised clustering methodologies are utilized for the segmentation of DFU [14]. Cascaded two steps SVM [15] and YOLOv3 are used to localize DFU [16]. The superpixel method [17], texture, color features [18] , and Cloud-based algorithms [19] are used to segment and classify the DFU. The handcrafted features are utilized for DFU classification which is selected manually, whereas in deep learning methodologies features extraction process is performed automatically [20]. Pre-trained CNN models are used for DFU detection [6], [21], [22]. The DFUnet is employed to classify the foot lesions into healthy/unhealthy classes [23]. The fully convolutional neural network [24], semantic segmentation model [25], are used for segmentation of the DFU [26]. Infrared thermography is a non-invasive technique [27] in which infrared thermal images are used to detect the DFU using different computer vision methodologies [28]. Smartphone health applications are becoming more popular to monitor the crucial aspects related to the human body [29], FootSnap application is used to create a standard DFU dataset [30] and MyFootCare gives suitable guidance related to the DFU patients. Few Apps facilitate the users to crop the patches of the images and also employ the color based clustering methodologies to segment the DFU [31], but these methods do not accurately segment the complete infected part of the human foot.

## III. PROPOSED METHODOLOGY

In this research methodology, 16 layers of the convolutional neural network is proposed to categorize the diabetic foot images into various pathological regions. The deep topographies are mined from the input images and supplied to the machine learning classifiers for screening the foot images. After screening, input images are further passed to the next proposed model YOLOv2-DFU which is designed by the combination of YOLOv2 [32] and shuffle net [33] for the localization of the abnormal region. The complete overview of the proposed architecture for DFU screening and localization is shown in Figure1.

### A. CLASSIFICATION OF DIABETIC FOOT ULCER

The proposed convolutional neural network model classifies the foot images into positive/negative and also provides help to find the image pattern to recognize the lesion symptoms. The proposed CNN model is trained on the diabetic foot images from scratch. In this model, convolutional layers are used with 5 × 5 filter sizes to activate the features in input images as depicted in Figure 2.

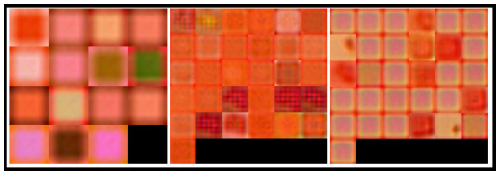


**FIGURE 2.** Convolutional layers (a) 1st (b) 2nd (c) 3rd.

The rectified linear activation units (ReLU) (shown in Figure 3) are used for fast training which maps the negative values with 0 and positive values with 1. The activated features are further passed to the batch normalization (Bn) layer.

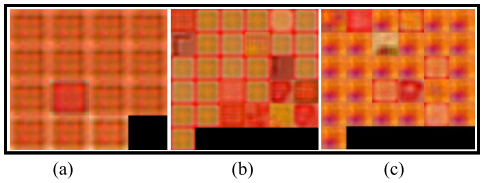


**FIGURE 3.** ReLU layers (a) 1st layer (b) 2nd layer (c) 3rd layer.

Three Bn layers are utilized between the ReLU and convolutional layers to minimize sensitivity and speed up the network training process. The batch-normalization is used for normalization by measuring the mean and variance across each input channel.

where ∈ is used to improve the numerical stability based on the variation of the mini-batch size as depicted in Figure 4.

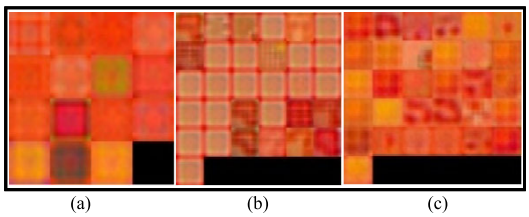


**FIGURE 4.** Batch-normalization layers (a) 1st layer (b) 2nd layer (c) 3rd layer.

The average pooling layer with 2 × 2 stride is used to simplify the output by non-linear down-sampling as shown in Figure 5.

Later, two fully connected (FC) layers are used, where input data is multiplied to the weight matrix and added with the bias as depicted in Figure 6.

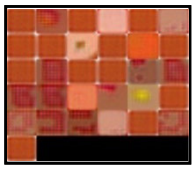

**FIGURE 5.** Pooling layer.

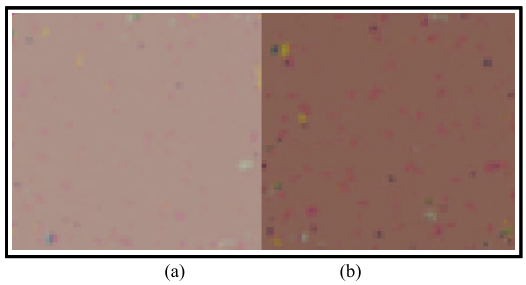


**FIGURE 6.** Fully connected layers (a) Fc1 (b) Fc2.

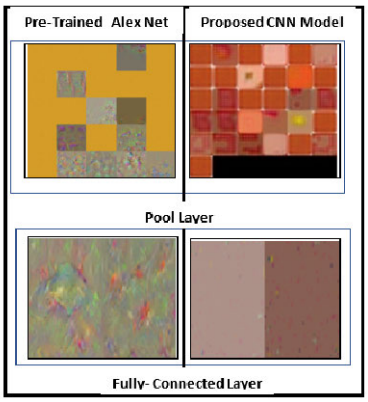


**FIGURE 7.** Features map comparison of proposed CNN model with existing pre-trained AlexNet model.

The features map of the proposed CNN model with existing pre-trained AlexNet model and DFU_QUTNet [22] is illustrated in the Figure 7-8.

In Figure 7-8, features map comparison shows that learning patterns contains highest information compared to existing CNN models. As shown in Figure 7-8, a proposed model extracts more significant features as compared to conventional pre-trained AlexNet and DFU_QUTNet [22] models. Figure 9 shows training procedure of the proposed network.

The proposed CNN architecture with activations is mentioned in Table 1.

In the proposed methodology, ReLU, and Batch- normalization layers are connected serially to learn the image patterns. The fully connected layers are used for feature mapping. Furthermore, softmax followed by the classification layer for the prediction of the foot lesions.

### B. LOCALIZATION OF DFU

YOLOv2 provides higher performance for object detection [35] in terms of speed and accuracy. In YOLOv2, extraction of candidate boxes & feature, target classification, and location steps are performed in a single unit. For accurate

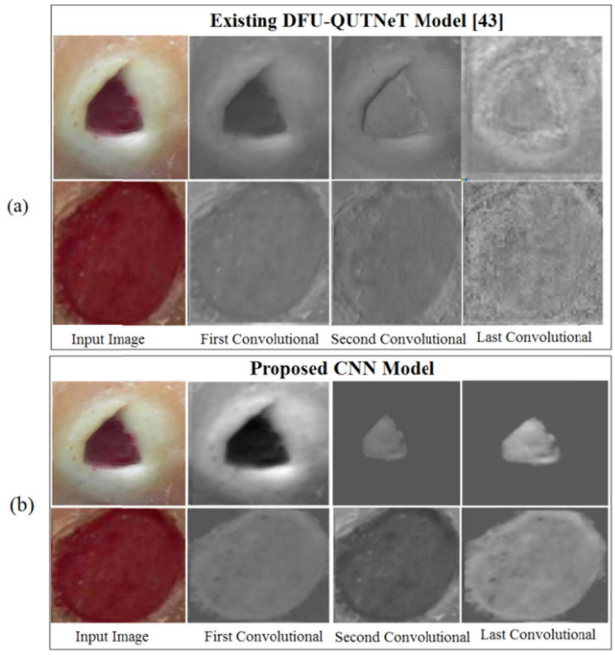


**FIGURE 8.** Features maps (a) features map of DFU_QUTNet [22] model (b) features map of the proposed model.

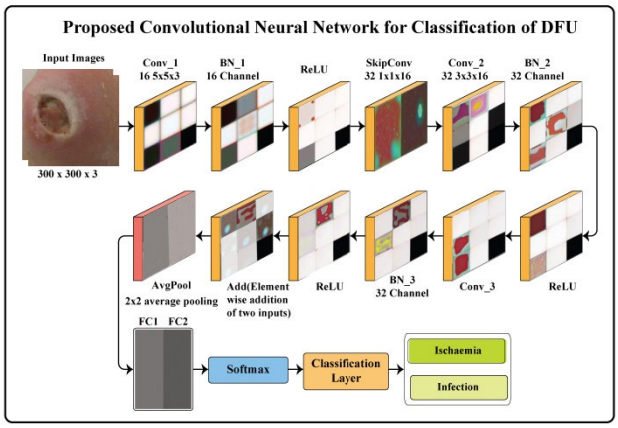


**FIGURE 9.** Network training procedure (Conv→ Convolution, BN→Batch-normalization, ReLU→ Rectified linear unit).

detection of DFU, the YOLOv2-DFU model is designed using YOLOv2 with a transfer learning model such as a shuffle net as a backbone.

### C. YOLOV2-DFU ARCHITECTURE

In this model, input images are passed to the shuffle-net, which contains 172 layers. The output of the shuffle-net at the ReLU node-199 layer is passed to the YOLOv2. YOLOv2 has Convolutional, ReLU, and batch-normalization layers which are serially connected and followed by YOLOv2 transform and YOLOv2output, which detects location with class labels of the infected regions in an input image more accurately. The proposed YOLOv2-DFU model is illustrated in Figure 10.

**TABLE 1.** PROPOSED CNN architecture with activation units.

| Layers | Size of the kernel with the stride | Activations |
|---|---|---|
| Input | 3 × 300 × 300 | 3 × 300 × 300 |
| conv_1 | 5 × 5 × 3, stride [1 1] | 300 × 300 × 16 |
| BN_1 | 16 channels | 300 × 300 × 16 |
| Relu_1 | 300 × 300 × 16 | - |
| skipConv | stride [2 2] | 150 × 150 × 32 |
| conv_2 | 3 × 3 × 16, stride [2 2] | 150 × 150 × 32 |
| BN_2 | 32 channels | 150 × 150 × 32 |
| Relu_2 | 150 × 150 × 32 | - |
| conv_3 | 3 × 3 × 32, stride [1 1] | 150 × 150 × 32 |
| BN_3 | 32 channels | 150 × 150 × 32 |
| Relu_3 | 150 × 150 × 32 | |
| Add | Element wise addition of two inputs | 150 × 150 × 32 |
| Avg pool | 2 × 2, stride [2 2] | 75 × 75 × 32 |
| FC | 2 FC | 1 × 1 × 2 |
| Softmax [34] | - | 1 × 1 × 2 |
| Categorical Cross - entropy [34] | Classification output | |

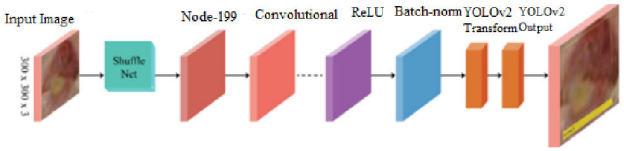


**FIGURE 10.** Proposed YOLOv2-DFU model.

YOLOv2-DFU model predicts the class labels using an anchor box as shown in Figure 11. The prediction is based on three major attributes [32]: (a) Intersection over the union (IOU) predicts score objectiveness across each anchor boxes, (b) Anchor box offset refines the position of the anchor boxes, (c) Class probability, predicts classes which are assigned to each anchor box.

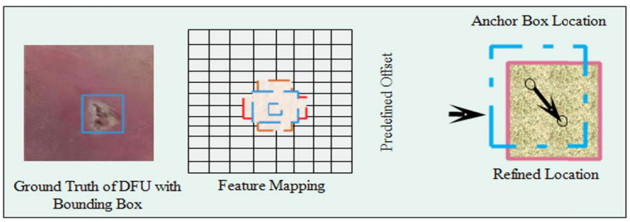


**FIGURE 11.** General working of YOLOv2 architecture.

In Figure 11, anchor boxes are shown by dotted colored lines at each feature mapped location which are refined by applying an offset. The class labels are predicted using color lines of the anchor boxes. The computational cost of the model depends on the input image size, in this model; 300 × 300 × 3 size of input images is used for training as well as testing. YOLOv2-DFU model is trained on three types of losses, i.e., localization loss, confidence loss, and classification loss to reduce mean squared error (MSE). The localization loss is computed using position and size of the predicted bounding box and the ground truth. Whereas, confidence loss indicates

objectness error i.e., object or no object detected in the predicted bounding box. The classification loss is computed as squared error between estimated and actual conditional probability. These losses are mathematically defined as:

$$\begin{aligned}&\text{Loss function}\\&= \lambda_1 \sum_{i=0}^{s^2} \sum_{j=0}^{B} 1_{ij}^{DFU}[(x_i - \hat{x_i})^2 + (y_i - \hat{y_i})^2]\\&+\lambda_1 \sum_{i=0}^{s^2} \sum_{j=0}^{B} 1_{i}^{DFU}[(\sqrt{\omega_i} - \sqrt{\hat{\omega_i}})^2+(\sqrt{h_i} - \sqrt{\hat{h_i}})^2]\\&+\lambda_2 \sum_{i=0}^{s^2} \sum_{j=0}^{B} 1_{ij}^{DFU}\\&\times[(c_i - \hat{c_i})^2 + \lambda_3 \sum_{i=0}^{s^2} \sum_{j=0}^{B} 1_{ij}^{NoDFU}\\&\times[(c_i - \hat{c_i})^2 + \lambda_4 \sum_{i=0}^{s^2} 1_{i}^{DFU} \sum_{c \in classes} (p_i(c) - \hat{p_i}(c))^2\end{aligned} \tag{1}$$

where $1_i^{DFU}$ denote input present in unit i and $1_{ij}^{DFU}$ denote jth predicted box in unit i in charge of the prediction, whereas s, h, $\omega$, c, p, $\lambda$, B represents the number of the grid cells, height, width, confidence scores, conditional class probability, weights, and bounding box respectively. $x_i$, $y_i$ represent the mid of the jth bounding box comparative to grid cell i and $\hat{x_i}$, $\hat{y_i}$ denote center of the ground truth relative to grid cell i.

## IV. RESULTS AND DISCUSSION

In this paper, two experiments have been performed for proposed method evaluation, first for classification of infection and ischemia, while second for the localization of infected regions that are obtained after classification.

### A. DATASET DESCRIPTION

DFU-Part (B) dataset is used for performance evaluation. The dataset contains infection and ischemia foot images. Ischemia data contains 4935 augmented negative and 4935 positive patches. The bacterial infection data contains augmented 2946 normal and 2946 abnormal skin patches [6], [23], [36]. The dataset description is mentioned in Table 2.

**TABLE 2. Dataset description.**

| Types | Classes | Cases | Patches | Augmentation |
|---|---|---|---|---|
| Ischaemia | **Absent(Normal** | 1249 | 1431 | 4935 |
| | **Present(Abnormal)** | 210 | 235 | 4935 |
| Bacterial infection | **Negative** | 628 | 684 | 2946 |
| | **Positive** | 831 | 982 | 2946 |

### B. Experiment#1 (Classification OF POSITIVE/NEGATIVE IMAGES OF DFU)

In this experiment, 0.5 hold out cross-validation, in which the model is trained on the randomly selected 50% data, and testing is performed on the remaining 50% data. The proposed method experiments are performed on Intel core i7, MATLAB 2020a with 740K Nvidia GPU.

**TABLE 3. Hyperparameters selection for the training of proposed CNN model.**

| Optimizer | Max Epochs | Validation Frequency | Learning Rate | Momentum | Mini Batch size | Accuracy |
|---|---|---|---|---|---|---|
| Stochastic gradient descent | 1000 | 80 | *0.001* | 0.8 | 8 | 0.87 |
| | | ***100*** | | ***0.9*** | ***16*** | ***0.99*** |
| | | 110 | | 0.1 | 64 | 0.85 |

**TABLE 4. Parameters of Machine learning classifiers.**

| DT | | KNN | | Ensemble | |
|---|---|---|---|---|---|
| Maximum number of splits | 100 | Number of neighbors | 1 | Ensemble method | AdaBoost |
| Split criteria | Gini diversity index | Distance metric | Euclidean Distance | Maximum number of splits | 200 |

The CNN training parameters are stated in the Table 3.

In Table 3, selected hyperparameters are highlighted in italic and bold those are used for further experimentation. The empirical outcomes are computed using Naive Bayes (NB) with Gaussian kernel [37], [38], Decision tree (DT) [39], Softmax [34], Ensemble [34] and K-nearest neighbor (KNN) classifiers [40]. The description of each classifier is mentioned in Table 4.

The classification results are presented in Table 5-6 and Figure 12.

**TABLE 5. Classification results on Ischaemia detection.**

| Classifiers | Sensitivity (SE) | Specificity (SP) | Accuracy (ACC) |
|---|---|---|---|
| NB | 0.979 | 0.978 | 0.979 |
| DT | 0.884 | 0.995 | 0.948 |
| Softmax | 1.00 | 0.962 | 0.976 |
| Ensemble | 0.840 | 0.752 | 0.772 |
| KNN | 0.889 | 1.00 | 0.952 |

**TABLE 6. Classification results on Infection detection.**

| Classifiers | SE | SP | ACC |
|---|---|---|---|
| NB | 0.250 | 0.945 | 0.932 |
| DT | 0.967 | 0.998 | 0.996 |
| Softmax | 0.930 | 0.969 | 0.943 |
| Ensemble | 1.00 | 0.976 | 0.977 |
| KNN | 0.531 | 0.969 | 0.943 |

In Table 5, achieved ischaemia screening accuracy results are 0.979, 0.948, 0.976, 0.772, 0.952 on NB, DT, Softmax, Ensemble, and KNN respectively, which shows that NB outperforms as compared to other classifiers having 0.979 accuracy. Similarly, in the infection screening process, achieved results are 0.932, 0.996, 0.943, 0.977, and 0.943 on NB, DT, Softmax, Ensemble, and KNN classifiers respectively, where DT achieves the highest accuracy to classify the positive/negatives images of the DFU. This set of experiments

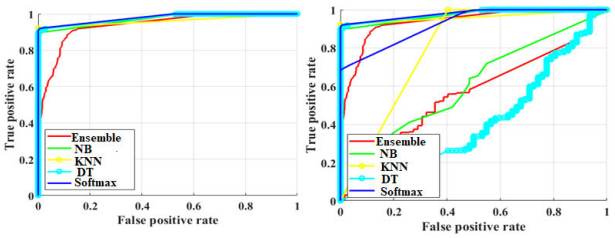


**FIGURE 12.** ROC (a) Infection (b) Ischaemia.

concludes that DT and NB performed better to classify the infection and ischaemia images respectively.

### C. PROPOSED DEEP LEARNING MODEL USING GRAD-CAM

Gradient-weighted class activation mapping (Grad-Cam) is the generalization form of the CAM method, where required computation is performed by automated gradient differentiation function. Grad-Cam uses a trained network, to visualize the input image features a score with the class label by incorporating weights of the last CNN layer as shown in Figure 13.

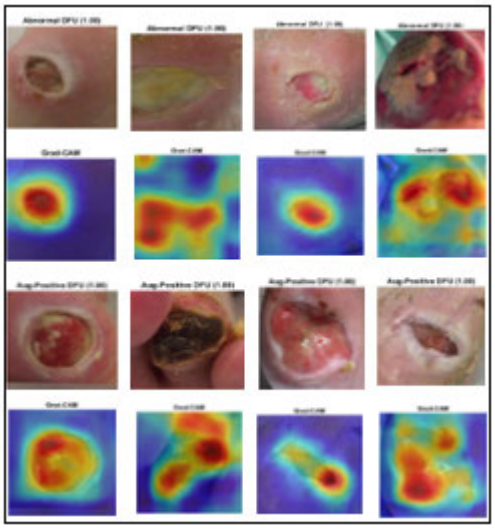

**FIGURE 13.** Input image with classification scores of the abnormal and positive class label.

The results in Figure 13 reflect that the proposed model accurately classifies the DFU. In this process, a total of eight images are tested, four from each ischaemia and infection classes on the trained model. Based on the Grad-CAM decisions using the trained network 1.00 score is achieved in all cases of the ischaemia and the infection. Why the model classifies better is discussed in section XI.

### D. GRAD-CAM EXPLAINS WHY

Grad-CAM is used to measure gradient of the categorization notch related to the concluding CNN layer of the network. This gradient is big in exact places where score mostly depends upon the data. The Grad-CAM function generates the map for a deep learning network, where computed derivative of the softmax score of the class label is related to the convolutional feature map. In automated differentiation, input images are converted into an array, and scores are measured by the Grad-CAM function. The selected classification (golden retriever) is performed based on the score and at the same time, automated differentiation is also utilized to compute the gradient of the final score with weights of the last CNN layer. In the previous section, Grad-CAM is used to compute the classification scores with the class label (Figure 12) while in this section the high-level features of the infected region with Alpha data of 0.5 values are plotted to visually represent the levels of the Grad-CAM.

In Figure 12, lowest and highest values are depicted by blue and red respectively and at the time the red color highlights the defected region clearly.

The achieved screening results of the DFU are also compared with recent methodologies [6], [21], [22], [41] in the Table 7.

**TABLE 7.** Comparison results of proposed method with existing methodologies ON Lancashire Teaching Hospital (LTH) DATASET.

| Ref | Year | Results |
|---|---|---|
| [42] | 2018 | 0.92 accuracy on Ischaemia (abnormal) |
| [21] | 2019 | 0.91 mAP on Ischaemia (abnormal) |
| [37] | 2020 | 0.73 accuracy on infection<br>0.90 accuracy on Ischaemia (abnormal) |
| [43] | 2020 | 0.92 sensitivity on Ischaemia (abnormal)[DFU_QUTNet]<br>0.92 [DFU_QUTNet+KNN]<br>0.93[DFU_QUTNet+SVM] |
| **Proposed method** | | 0.97 accuracy, 1.00 sensitivity on Ischaemia (abnormal)<br>0.99 accuracy on infection and 0.95 mAP on Ischaemia (abnormal) |

In the domain of DFU detection maximum achieved accuracy in literature is 0.73 and 0.90 for infection and ischaemia detection respectively. Whereas the proposed model achieved 0.99 and 0.97 accuracy on infection and ischaemia. The results comparison with current published work [6], [21], [22], [41]. In [6] handcrafted and deep features are extracted from pre-trained models of CNN such as ResNet50, Inception-V3, and InceptionRes-NetV2 whereas in [21] InceptionV2 is used for DFU classification. In addition, faster RCNN [6], [21], [42] is used to localize the infected regions. In proposed research methodology two deep learning models are proposed which are trained from the scratch, subsequently, a 16-layer CNN model is used for classification and the YOLOv2 model is used for localization which is lightweight and powerful as compared to faster-RCNN.

As compared with existing recent published work, proposed network is trained with sgdm (optimizer), and 0.001 learning rate. The proposed model precisely localized and classifies the affected foot region.

The proposed research methodology has shown much improved results compared to the existing methods [6], [21], [22], [41] in terms of classification and localization.

### E. EXPERIMENT#2 (LOCALIZATION OF THE ISCHAEMIA AND INFECTION)

YOLOv2-DFU architecture is developed for infected region of foot localization. The input images are divided into M × N grid, and detection is performed using each grid when infected region lie in center part of the grid cell. The initial bounding box B is given to each grid having different specifications. The predicted B is achieved (x, y, w, h) with confidence scores as define in Eq (2) for respective bounding boxes by deep CNN model.

$$\mathrm{c\,(DF)} = \mathrm{p\,(DFU)}\,.\mathrm{IOU}_{\mathrm{Prediction}}^{\mathrm{Truth}} \tag{2}$$

The score c (DF) defines class probability which belongs to truth bounding box and degree of the fitting among input and predicted bounding box.

$$\mathrm{IOU}_{\mathrm{Prediction}}^{\mathrm{Truth}} = \frac{\mathrm{Area(B\,(truthimages)} \cap B\,\mathrm{(prediction))}}{\mathrm{Area(B\,(truthimages)} \cup B\,\mathrm{(prediction))}} \tag{3}$$

Eq (3) defines as ratio among the interaction & union of ground truth and predicted B. The YOLO loss is computed by measuring the mean squared error among prediction and ground truth bounding boxes. The three types of loss functions (classification, localization, and confidence) are computed.

Localization loss calculates error among the predicted bounding box size and the location.

$$\lambda_1 \sum_{\mathrm{i}=0}^{\mathrm{s}^2} \sum_{\mathrm{j}=0}^{\mathrm{B}} 1_{\mathrm{ij}}^{\mathrm{DFU}} [(\mathrm{x_i} - \hat{x_i})^2 + (\mathrm{y_i} - \hat{y_i})^2 + \lambda_2 \times \sum_{\mathrm{i}=0}^{\mathrm{s}^2} \sum_{\mathrm{j}=0}^{\mathrm{B}} 1_{\mathrm{i}}^{\mathrm{DFU}} [(\omega_{\mathrm{i}} - \hat{\omega_i})^2 + \left(\mathrm{h_i} - \hat{h_i}\right)^2] \tag{4}$$

$$\sum_{\mathrm{i}=0}^{\mathrm{s}^2} \sum_{\mathrm{j}=0}^{\mathrm{B}} 1_{\mathrm{ij}}^{\mathrm{DFU}} [(\mathrm{c_i} - \hat{c_i})^2 \tag{5}$$

where $\hat{c_i}$ denotes the score of the B in s and $1_{\mathrm{ij}}^{\mathrm{DFU}}$ if j bounding box is responsible for the detection of DFU otherwise = 0. When DFU is not detected in B then confidence loss is measured as follows:

$$\lambda_3 \sum_{\mathrm{i}=0}^{\mathrm{s}^2} \sum_{\mathrm{j}=0}^{\mathrm{B}} 1_{\mathrm{ij}}^{\mathrm{noDFU}} [(\mathrm{c_i} - \hat{c_i})^2 \tag{6}$$

where $1_{\mathrm{ij}}^{\mathrm{noDFU}}$ is the complement of the $1_{\mathrm{ij}}^{\mathrm{DFU}}$ and $\lambda_3$ loss weight is decreased when the background is detected. In classification loss, DFU is detected to compute the conditional class probabilities across each class in s that is defined as:

$$\lambda_4 \sum_{\mathrm{i}=0}^{\mathrm{s}^2} 1_{\mathrm{i}}^{\mathrm{DFU}} \sum_{\mathrm{c} \in \mathrm{classes}} (\mathrm{p_i\,(c)} - \hat{p_i}\,\mathrm{(c)})^2 \tag{7}$$

where $1_{\mathrm{i}}^{\mathrm{DFU}} = 1$ when DFU is present otherwise 0 and $\hat{p_i}$ (c) denote the probability for each class in s. The proposed model is trained on 40 epochs, as depicted in Figure 14. The proposed YOLOv2-DFU model is trained on different parameters as mentioned in the Table 8. The empirical results

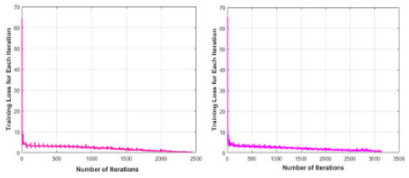

(a) (b)

**FIGURE 14.** Training loss across each iterations (a) Ischaemia (b) Infection.

**TABLE 8.** TRAINING parameters of proposed YOLOv2-DFU model.

| MaxEpochs | Shuffle | Validation Frequency | Learning Rate |
|---|---|---|---|
| 40 | Every epoch | 10 | 0.001 |

**TABLE 9.** Localization results in term of mean IOU on 50% training cases.

| Dataset | Mean IOU on Ischaemia | Mean IOU on Infection |
|---|---|---|
| Proposed work | 0.98 | 0.97 |

have been computed using different performance metrics for infection and ischaemia localization such as IOU, precision, log average miss rate, and recall. The Mean IOU is computed on the benchmark datasets as mentioned in Table 9.

In Table 9, achieved results are 0.98 IOU on Ischaemia and 0.97 IOU on Infection to localize the abnormal foot region. Furthermore, the mean IOU across the number of the anchor box is graphically shown in Figure 15.

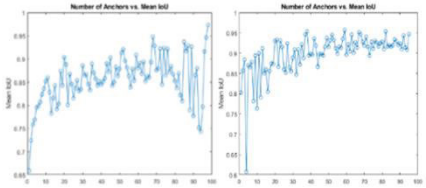

(a) (b)

**FIGURE 15.** MeanIOU of DFU detection (a) Ischaemia (b) Infection.

Figure 16-17, shows exact location of the infected region is localized with confidence scores.

The visually presented results in Figure 16 shows that the proposed method achieves a maximum 0.973 confidence score to localize the abnormal foot region. While Figure 17 results show that the proposed method obtains 0.963 confidence scores for the detection of the positive region of the DFU. The quantitative and visually represented results in the (Figure 15-16) shows that the proposed model performs better to localize the actual infected region of the foot. The precision and recall measures are also computed image by image as mentioned in Table 10. The mean of average precision (mAP) and log average miss rate (LAma) are computed as mentioned in Table 11.

**TABLE 10.** Quantitative results on benchmark dataset.

| Ischaemia | | | Infection | | |
|---|---|---|---|---|---|
| Image Name | Precision | Recall | No of images | Precision | Recall |
| 2.03_138.jpg | 0.979 | 0.900 | Aug-Positive-001125_20.jpg | 0.952 | 0.900 |
| 2.03_140.jpg | 0.980 | 0.905 | Aug-Positive-001125_30.jpg | 0.955 | 0.905 |
| 2.03_141.jpg | 0.980 | 0.905 | Aug-Positive-001127_11.jpg | 0.956 | 0.905 |
| 2.03_142.jpg | 0.987 | 0.906 | Aug-Positive\001127_21.jpg | 0.958 | 0.906 |
| 2.03_143.jpg | 0.987 | 0.900 | Aug-Positive\001127_31.jpg | 0.960 | 0.900 |
| 2.03_145.jpg | 0.984 | 0.901 | Aug-Positive\001129_11.jpg | 0.961 | 0.901 |
| 2.03_146.jpg | 0.982 | 0.903 | Aug-Positive\001129_21.jpg | 0.962 | 0.903 |
| 2.03_147.jpg | 0.986 | 0.909 | Aug-Positive\001129_31.jpg | 0.964 | 0.909 |
| 2.03_149.jpg | 0.987 | 0.906 | Aug-Positive\001135_11.jpg | 0.960 | 0.906 |
| 2.03_150.jpg | 0.989 | 0.908 | Aug-Positive\001135_21.jpg | 0.967 | 0.908 |
| 2.03_155.jpg | 0.984 | 0.903 | Aug-Positive\001135_31.jpg | 0.961 | 0.903 |
| 2.03_157.jpg | 0.983 | 0.906 | Aug-Positive\001137_11.jpg | 0.960 | 0.906 |
| 2.03_158.jpg | 0.981 | 0.901 | Aug-Positive\001137_21.jpg | 0.967 | 0.901 |
| 2.03_161.jpg | 0.983 | 0.906 | Aug-Positive\001137_31.jpg | 0.970 | 0.906 |
| 2.03_162.jpg | 0.989 | 0.918 | Aug-Positive\001138_10.jpg | 0.971 | 0.909 |
| 2.03_163.jpg | 0.980 | 0.904 | Aug-Positive\001138_20.jpg | 0.972 | 0.904 |
| 2.03_164.jpg | 0.983 | 0.906 | Aug-Positive\001138_30.jpg | 0.973 | 0.906 |
| 2.03_165.jpg | 0.985 | 0.905 | Aug-Positive\001139_11.jpg | 0.976 | 0.905 |
| 2.03_167.jpg | 0.983 | 0.901 | Aug-Positive\001139_21.jpg | 0.974 | 0.901 |
| 2.03_168.jpg | 0.984 | 0.902 | Aug-Positive\001139_31.jpg | 0.975 | 0.902 |
| 2.03_169.jpg | 0.987 | 0.902 | Aug-Positive\001140_10.jpg | 0.971 | 0.902 |
| 2.03_170.jpg | 0.982 | 0.905 | Aug-Positive\001140_20.jpg | 0.976 | 0.905 |
| 2.03_171.jpg | 0.989 | 0.908 | Aug-Positive\001140_30.jpg | 0.974 | 0.908 |
| 2.03_172.jpg | 0.981 | 0.904 | Aug-Positive\001141_10.jpg | 0.977 | 0.904 |
| 2.03_174.jpg | 0.984 | 0.907 | Aug-Positive\001141_20.jpg | 0.978 | 0.907 |
| 2.03_177.jpg | 0.983 | 0.902 | Aug-Positive\001141_30.jpg | 0.972 | 0.902 |
| 2.03_178.jpg | 0.986 | 0.907 | Aug-Positive\001142_10.jpg | 0.979 | 0.907 |
| 2.03_179.jpg | 0.980 | 0.975 | Aug-Positive\001142_20.jpg | 0.976 | 0.975 |
| 2.03_181.jpg | 0.989 | 0.943 | Aug-Positive\001142_30.jpg | 0.974 | 0.943 |
| 2.03_182.jpg | 0.987 | 0.987 | Aug-Positive\001143_10.jpg | 0.980 | 0.987 |
| 2.03_184.jpg | 0.989 | 0.952 | Aug-Positive\001143_20.jpg | 0.985 | 0.952 |
| 2.03_185.jpg | 0.980 | 0.917 | Aug-Positive\001143_30.jpg | 0.981 | 0.917 |
| 2.03_188.jpg | 0.984 | 0.955 | Aug-Positive\001144_10.jpg | 0.988 | 0.955 |
| 2.03_190.jpg | 0.907 | 0.983 | Aug-Positive\001144_20.jpg | 0.982 | 0.983 |
| 2.03_193.jpg | 0.981 | 0.967 | Aug-Positive\001144_30.jpg | 0.982 | 0.967 |
| 2.03_196.jpg | 0.982 | 0.923 | Aug-Positive\001145_11.jpg | 0.987 | 0.923 |
| 2.03_197.jpg | 0.987 | 0.906 | Aug-Positive\001145_21.jpg | 0.984 | 0.906 |
| 2.03_198.jpg | 0.983 | 0.977 | Aug-Positive\001145_31.jpg | 0.982 | 0.977 |
| 2.03_199.jpg | 0.987 | 0.966 | Aug-Positive\001148_10.jpg | 0.983 | 0.966 |
| 2.03_202.jpg | 0.986 | 0.907 | Aug-Positive\001148_20.jpg | 0.983 | 0.907 |
| 2.03_203.jpg | 0.984 | 0.944 | Aug-Positive\001148_30.jpg | 0.986 | 0.944 |
| 2.03_205.jpg | 0.988 | 0.909 | Aug-Positive\001149_10.jpg | 0.988 | 0.909 |
| 2.03_206.jpg | 0.980 | 0.909 | Aug-Positive\001149_20.jpg | 0.981 | 0.909 |
| 2.03_207.jpg | 0.981 | 0.974 | Aug-Positive\001152_10.jpg | 0.989 | 0.974 |
| 2.03_208.jpg | 0.987 | 0.940 | Aug-Positive\001152_20.jpg | 0.981 | 0.940 |
| 2.03_209.jpg | 0.980 | 0.914 | Aug-Positive\001152_30.jpg | 0.986 | 0.914 |
| 2.03_211.jpg | 0.986 | 0.910 | Aug-Positive\001153_10.jpg | 0.985 | 0.910 |
| 2.03_215.jpg | 0.983 | 0.987 | Aug-Positive\001153_20.jpg | 0.986 | 0.987 |
| 2.03_220.jpg | 0.987 | 0.973 | Aug-Positive\001153_30.jpg | 0.986 | 0.973 |
| 2.03_221.jpg | 0.988 | 0.940 | Aug-Positive\001154_10.jpg | 0.986 | 0.940 |
| 2.03_225.jpg | 0.989 | 0.987 | Aug-Positive\001154_20.jpg | 0.986 | 0.987 |
| 2.03_226.jpg | 0.995 | 0.970 | Aug-Positive\001154_30.jpg | 0.988 | 0.970 |
| 2.03_229.jpg | 0.990 | 0.997 | Aug-Positive\001158_10.jpg | 0.987 | 0.997 |
| 2.03_233.jpg | 0.993 | 0.960 | Aug-Positive\001158_20.jpg | 0.987 | 0.96 |
| 2.03_234.jpg | 0.992 | 0.997 | Aug-Positive\001158_30.jpg | 0.989 | 0.997 |
| 2.03_235.jpg | 0.998 | 0.950 | Aug-Positive\001159_10.jpg | 0.980 | 0.950 |
| 2.03_240.jpg | 0.994 | 0.945 | Aug-Positive\001159_12.jpg | 0.984 | 0.945 |

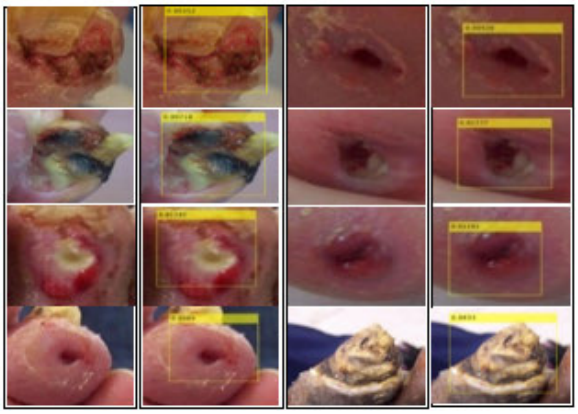


**FIGURE 16.** Infection detection (a), (c) original DFU images (b), (d) score of the confidence.

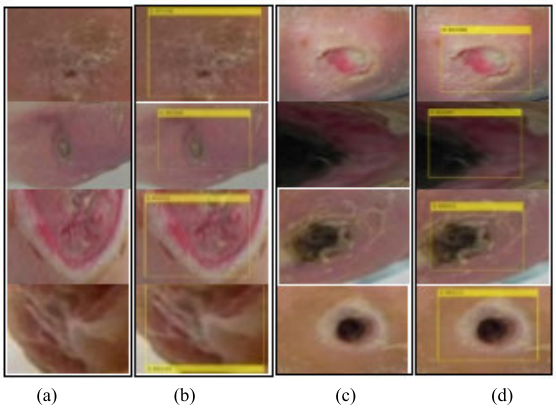


**FIGURE 17.** Ischaemia detection (a), (c) original DFU images (b), (d) score of the confidence.

**TABLE 11.** Average the proposed Approach Results on 50% training cases.

| Ischaemia | | Infection | |
|---|---|---|---|
| mAP | LAma | mAP | LAma |
| 0.95 | 0.1 | 0.90 | 0.3 |

In Table 11, results are analyzed in terms of the mean of the recall and precision, which shows that the detection

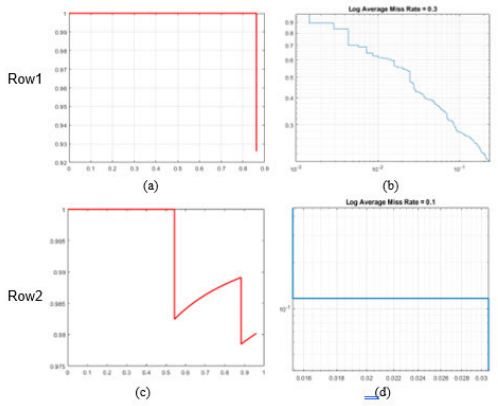


**FIGURE 18.** Average results of the proposed method (a, c) average precision and the recall curve (b, d) LAma (where Row1 shows infection results and Row 2 shows ischaemia results).

results are 0.95mAP on ischaemia, and 0.90mAP on the infection. The overall localization experiment concludes that the YOLOv2-DFU model achieved a higher precision rate to localize the ischaemia as compared to the infection. The mRP and LAma are plotted in Figure 18.

In Figure 18, the average results are 0.90 mAP and 0.3 average miss rate on infection, while 0.95 mAP and 0.1 average miss rate on ischaemia dataset. The proposed method results are associated with current methods as given in the Table 12. Table 12, presents the localization results of the existing YOLOv2 model as well as modified YOLOv2 model, where ShuffleNet is used as a backbone of the YOLOv2, in which proposed method achieved better results as compared to existing method.

The localization results are analyzed with different ratio of the training and validation dataset, where we observed that proposed approach outperform only 10% training dataset. Furthermore, proposed method results are visually represented in the Figure 19. Visually presented results in the Figure 19, shows that proposed method achieved 0.94 and 0.95 localization scores on modified YOLOv2 model whereas, 0.75 and 0.86 localization scores on existing YOLOv2 model. The experimental result clearly shows the proposed technique contribution.

**TABLE 12.** Comparison of the proposed method results.

| Dataset | Modified YOLOv2 | YOLOv2 |
|---|---|---|
| 50% training data | 0.96 mAp on Ischaemia<br>0.92 mAp on infection | 0.75 mAp on Ischaemia<br>0.69 mAp on infection |
| 50% validation data | 0.95 mAp on Ischaemia<br>0.90 mAp on infection | 0.71 mAp on Ischaemia<br>0.62 mAp on infection |
| 10% training data | 0.98 mAp on Ischaemia<br>0.93 mAp on infection | 0.75 mAp on Ischaemia<br>0.68 mAp on infection |
| 10% validation data | 1.00 mAP on Ischaemia and infection | 0. 79 mAp on Ischaemia<br>0.74 mAp on infection |

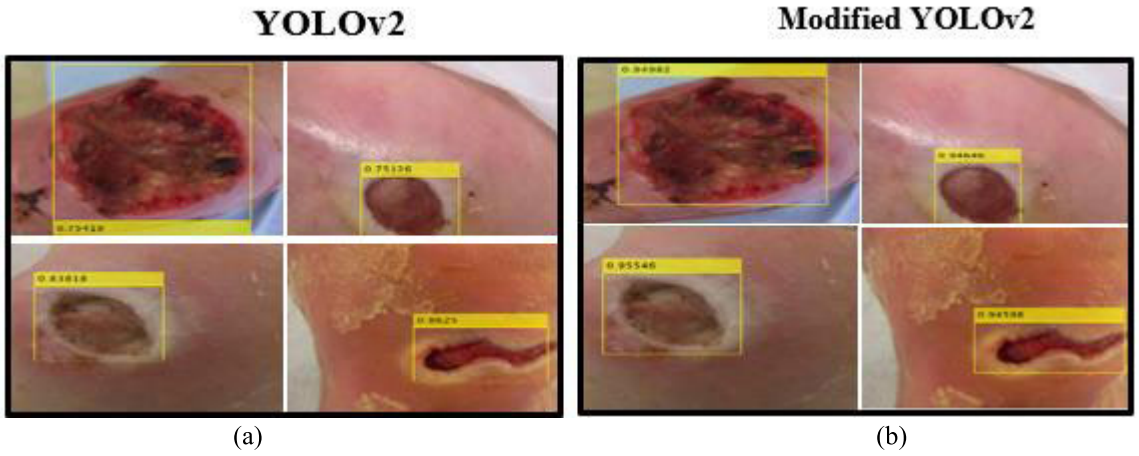


**FIGURE 19.** Comparison of proposed method results (a) YOLOv2 (b) modified YOLOv2.

## V. CONCLUSION

In this work, deep learning approaches are presented for localization and classification of DFU. The 16 layers proposed CNN model performs better because classification results depend upon the combination of the selected convolutional layers. For localization, the YOLOv2-DFU model is designed by using a shuffle net as a backbone of the YOLOv2. The localization results proved that a combination of the shuffle net and the YOLOv2 model is more effective to localize the infected region of the foot images. Finlay, this research will provide an open research area for the researcher to use this method as it is or fine-tune it to localize the infected region of the different body parts such as the brain, lung, and stomach, etc. Overall, it is concluded that the proposed approach is unique, novel, and more helpful to classify & localize the DFU more accurately.

## VI. FUTURE WORK

The proposed method classifies the DFU into two classes such as normal/abnormal. In the upcoming tasks, we aim to extend the DFU classification method by using the unsupervised reinforcement learning to classify the different grades of DFU such as grades 0, 1, 2, 3, and 4. The dermatologists can use this work to diagnose the infection and ischaemia at an initial stage that in turn will improve the treatment process and increase the patient survival rate.

## REFERENCES

[1] B. Shabbir, M. Sharif, W. Nisar, M. Yasmin, and S. L. Fernandes, "Automatic cotton wool spots extraction in retinal images using texture segmentation and Gabor wavelet," *J. Integr. Design Process Sci.*, vol. 20, no. 1, pp. 65–76, Jun. 2016.

[2] R. J. Snyder, R. S. Kirsner, R. A. Warriner, III, L. A. Lavery, J. R. Hanft, and P. Sheehan, *Consensus Recommendations on Advancing the Standard of Care for Treating Neuropathic Foot Ulcers in Patients With Diabetes*, vol. 56, no. 4. Devault, PA, USA: HMP Communications, 2010, p. S1.

[3] H. K. Eltzschig and T. Eckle, "Ischemia and reperfusion—From mechanism to translation," *Nature Med.*, vol. 17, no. 11, p. 1391, 2011.

[4] R. Ikem, I. Ikem, O. Adebayo, and D. Soyoye, "An assessment of peripheral vascular disease in patients with diabetic foot ulcer," *Foot*, vol. 20, no. 4, pp. 114–117, Dec. 2010.

[5] B. Peter-Riesch, "The diabetic foot: The never-ending challenge," in *Novelties in Diabetes*, vol. 31. Berlin, Germany: Karger, 2016, pp. 108–134.

[6] M. Goyal, N. D. Reeves, S. Rajbhandari, N. Ahmad, C. Wang, and M. H. Yap, "Recognition of ischaemia and infection in diabetic foot ulcers: Dataset and techniques," *Comput. Biol. Med.*, vol. 117, Feb. 2020, Art. no. 103616.

[7] J. D. Peter, S. L. Fernandes, C. E. Thomaz, and S. Viriri, *Computer Aided Intervention and Diagnostics in Clinical and Medical Images*. Cham, Switzerland: Springer, 2019.

[8] J. Amin, M. Sharif, M. Yasmin, T. Saba, M. A. Anjum, and S. L. Fernandes, "A new approach for brain tumor segmentation and classification based on score level fusion using transfer learning," *J. Med. Syst.*, vol. 43, no. 11, p. 326, Nov. 2019.

[9] C. Kang, X. Yu, S. H. Wang, D. Guttery, H. Pandey, Y. Tian, and Y. Zhang, "A heuristic neural network structure relying on fuzzy logic for images scoring," *IEEE Trans. Fuzzy Syst.*, early access, Jan. 13, 2020, doi: 10.1109/TFUZZ.2020.2966163.

[10] S. Wang, J. Sun, I. Mehmood, C. Pan, Y. Chen, and Y. Zhang, "Cerebral micro-bleeding identification based on a nine-layer convolutional neural network with stochastic pooling," *Concurrency Comput., Pract. Exper.*, vol. 32, no. 1, p. e5130, Jan. 2020.

[11] S. Wang, C. Tang, J. Sun, and Y. Zhang, "Cerebral micro-bleeding detection based on densely connected neural network," *Frontiers Neurosci.*, vol. 13, p. 422, May 2019.

[12] P. C. Leung, "Diabetic foot ulcers—A comprehensive review," *Surgeon*, vol. 5, no. 4, pp. 219–231, Aug. 2007.

[13] G. D. Valk, D. Kriegsman, and W. Assendelft, "Patient education for preventing diabetic foot ulceration. A systematic review," *Endocrinol. Metabolism Clinics North Amer.*, vol. 31, no. 3, pp. 633–658, 2002.

[14] H. D. Cheng, X. H. Jiang, Y. Sun, and J. Wang, "Color image segmentation: Advances and prospects," *Pattern Recognit.*, vol. 34, no. 12, pp. 2259–2281, Dec. 2001.

[15] L. Wang, P. C. Pedersen, E. Agu, D. M. Strong, and B. Tulu, "Area determination of diabetic foot ulcer images using a cascaded two-stage SVM-based classification," *IEEE Trans. Biomed. Eng.*, vol. 64, no. 9, pp. 2098–2109, Sep. 2017.

[16] A. Han, Y. Zhang, A. Li, C. Li, F. Zhao, Q. Dong, Q. Liu, Y. Liu, X. Shen, S. Yan, and S. Zhou, "Efficient refinements on YOLOv3 for real-time detection and assessment of diabetic foot Wagner grades," 2020, *arXiv:2006.02322*. [Online]. Available: https://arxiv.org/abs/2006.02322

[17] G. Blanco, A. J. M. Traina, C. Traina, Jr., P. M. Azevedo-Marques, A. E. S. Jorge, D. de Oliveira, and M. V. N. Bedo, "A superpixel-driven deep learning approach for the analysis of dermatological wounds," *Comput. Methods Programs Biomed.*, vol. 183, Jan. 2020, Art. no. 105079.

[18] S. Patel, R. Patel, and D. Desai, "Diabetic foot ulcer wound tissue detection and classification," in *Proc. Int. Conf. Innov. Inf., Embedded Commun. Syst. (ICIIECS)*, Mar. 2017, pp. 1–5.

[19] B. Cassidy, N. D. Reeves, P. Joseph, D. Gillespie, C. O'Shea, S. Rajbhandari, A. G. Maiya, E. Frank, A. Boulton, D. Armstrong, B. Najafi, J. Wu, M. H. Yap, "DFUC2020: Analysis towards diabetic foot ulcer detection," 2020, *arXiv:2004.11853*. [Online]. Available: https://arxiv.org/abs/2004.11853
[20] C. Wang, X. Yan, M. Smith, K. Kochhar, M. Rubin, S. M. Warren, J. Wrobel, and H. Lee, "A unified framework for automatic wound segmentation and analysis with deep convolutional neural networks," in *Proc. 37th Annu. Int. Conf. IEEE Eng. Med. Biol. Soc. (EMBC)*, Aug. 2015, pp. 2415–2418.
[21] M. Goyal, N. D. Reeves, S. Rajbhandari, and M. H. Yap, "Robust methods for real-time diabetic foot ulcer detection and localization on mobile devices," *IEEE J. Biomed. Health Informat.*, vol. 23, no. 4, pp. 1730–1741, Jul. 2019.
[22] L. Alzubaidi, M. A. Fadhel, S. R. Oleiwi, O. Al-Shamma, and J. Zhang, "DFU_QUTNet: Diabetic foot ulcer classification using novel deep convolutional neural network," *Multimedia Tools Appl.*, vol. 79, nos. 21–22, pp. 15655–15677, Jun. 2020.
[23] M. Goyal, N. D. Reeves, A. K. Davison, S. Rajbhandari, J. Spragg, and M. H. Yap, "DFUNet: Convolutional neural networks for diabetic foot ulcer classification," *IEEE Trans. Emerg. Topics Comput. Intell.*, vol. 4, no. 5, pp. 728–739, Oct. 2020.
[24] M. Goyal, M. H. Yap, N. D. Reeves, S. Rajbhandari, and J. Spragg, "Fully convolutional networks for diabetic foot ulcer segmentation," in *Proc. IEEE Int. Conf. Syst., Man, Cybern. (SMC)*, Oct. 2017, pp. 618–623.
[25] M. Goyal, M. Hoon Yap, and S. Hassanpour, "Multi-class semantic segmentation of skin lesions via fully convolutional networks," 2017, *arXiv:1711.10449*. [Online]. Available: http://arxiv.org/abs/1711.10449
[26] M. Goyal, J. Ng, and M. Hoon Yap, "Multi-class lesion diagnosis with pixel-wise classification network," 2018, *arXiv:1807.09227*. [Online]. Available: http://arxiv.org/abs/1807.09227
[27] B. B. Lahiri, S. Bagavathiappan, T. Jayakumar, and J. Philip, "Medical applications of infrared thermography: A review," *Infr. Phys. Technol.*, vol. 55, no. 4, pp. 221–235, Jul. 2012.
[28] L. Fraiwan, M. AlKhodari, J. Ninan, B. Mustafa, A. Saleh, and M. Ghazal, "Diabetic foot ulcer mobile detection system using smart phone thermal camera: A feasibility study," *Biomed. Eng. OnLine*, vol. 16, no. 1, p. 117, Dec. 2017.
[29] S. Kacmaz, E. Ercelebi, S. Zengin, and S. Cindoruk, "The use of infrared thermal imaging in the diagnosis of deep vein thrombosis," *Infr. Phys. Technol.*, vol. 86, pp. 120–129, Nov. 2017.
[30] M. H. Yap, C.-C. Ng, K. Chatwin, C. A. Abbott, F. L. Bowling, A. J. M. Boulton, and N. D. Reeves, "Computer vision algorithms in the detection of diabetic foot ulceration: A new paradigm for diabetic foot care?" *J. Diabetes Sci. Technol.*, vol. 10, no. 2, pp. 612–613, Mar. 2016.
[31] B. Ploderer, R. Brown, L. S. D. Seng, P. A. Lazzarini, and J. J. van Netten, "Promoting self-care of diabetic foot ulcers through a mobile phone app: User-centered design and evaluation," *JMIR Diabetes*, vol. 3, no. 4, Oct. 2018, Art. no. e10105.
[32] J. Redmon and A. Farhadi, "YOLO9000: Better, faster, stronger," in *Proc. IEEE Conf. Comput. Vis. Pattern Recognit. (CVPR)*, Jul. 2017, pp. 7263–7271.
[33] X. Zhang, X. Zhou, M. Lin, and J. Sun, "ShuffleNet: An extremely efficient convolutional neural network for mobile devices," in *Proc. IEEE/CVF Conf. Comput. Vis. Pattern Recognit.*, Jun. 2018, pp. 6848–6856.
[34] C. M. Bishop, *Pattern Recognition and Machine Learning*. New York, NY, USA: Springer 2006.
[35] J. Redmon and A. Farhadi, "YOLO9000: Better, faster, stronger," in *Proc. IEEE Conf. Comput. Vis. Pattern Recognit. (CVPR)*. Piscataway, NJ, USA: IEEE Press, 2017. Accessed: Feb. 19, 2020. [Online]. Available: https://medium.com/jonathan_hui/real-time-object-detection-with-yolo-yolov2-28b1b93e2088
[36] M. Goyal, N. D. Reeves, S. Rajbhandari, and M. H. Yap, "Robust methods for real-time diabetic foot ulcer detection and localization on mobile devices," *IEEE J. Biomed. Health Informat.*, vol. 23, no. 4, pp. 1730–1741, Jul. 2019.
[37] T. Hastie, R. Tibshirani, and J. Friedman, *The Elements of Statistical Learning: Data Mining, Inference, and Prediction*. New York, NY, USA: Springer, 2009.
[38] H. Schütze, C. D. Manning, and P. Raghavan, *Introduction to Information Retrieval*. Cambridge, U.K.: Cambridge Univ. Press, 2008.
[39] L. Breiman, J. Friedman, C. J. Stone, and R. A. Olshen, *Classification and Regression Trees*. Boca Raton, FL, USA: CRC Press, 1984.
[40] M. H. A. Abdullah, M. Othman, S. Kasim, S. S. Saharuddin, and S. A. Mohamed, "A spiking neural networks model with fuzzy-weighted K-nearest neighbour classifier for real-world flood risk assessment," in *Proc. Int. Conf. Soft Comput. Data Mining*. Cham, Switzerland: Springer, 2020, pp. 222–230.
[41] M. Goyal, N. D. Reeves, A. K. Davison, S. Rajbhandari, J. Spragg, and M. H. Yap, "Dfunet: Convolutional neural networks for diabetic foot ulcer classification," *IEEE Trans. Emerg. Topics Comput. Intell.*, vol. 4, no. 5, pp. 728–739, Oct. 2020.
[42] A. L. da Costa Oliveira and D. O. Dantas, "Faster R-CNN approach for diabetic foot ulcer detection," Dept. Comput., Univ. Federal de Sergipe, São Cristóvão, Brazil, pp. 1–10. Accessed: Dec. 18, 2020. [Online]. Available: http://grand-challengepublic.s3.amazonaws.com/evaluation-supplementary/532/3c68e2c6-c6bd-456ebe40-68e11d5c3f6a/Faster_RCNN_DFU.pdf
[43] N. Rania, H. Douzi, L. Yves, and T. Sylvie, "Semantic segmentation of diabetic foot ulcer images: Dealing with small dataset in DL approaches," in *Proc. Int. Conf. Image Signal Process.* Cham, Switzerland: Springer, 2020, pp. 162–169.
[44] M. Goyal and S. Hassanpour, "A refined deep learning architecture for diabetic foot ulcers detection," 2020, *arXiv:2007.07922*. [Online]. Available: http://arxiv.org/abs/2007.07922

**JAVARIA AMIN** actively involved in research and producing high-quality work on Medical Image Processing, Pattern Recognition, and Computer Vision. She has published more than 22 research articles in reputed and prestigious international journals with an accumulated impact factor of around 55. Her research interests include the detection of anomalies in human body parts using machine learning and powerful deep learning algorithms.

**MUHAMMAD SHARIF** (Senior Member, IEEE) is currently an Associate Professor with COMSATS University Islamabad–Wah, Pakistan. He has worked one year in Alpha Soft UK based software house in 1995. He is also the OCP in Developer Track. He has been in teaching profession since 1996 to date. His research interests include medical imaging, biometrics, computer vision, machine learning, and agriculture plants imaging. He has been being awarded with COMSATS Research Productivity Award since 2011 till 2018. He has served in TPC for IEEE FIT 2014–2019. He is also serving as an Associate Editor for IEEE Access, a Guest Editor of Special Issues, and a reviewer for well reputed journals. He also headed the department from 2008 to 2011 and achieved the targeted outputs. He has more than 210 research publications in IF, SCI, and ISI journals as well as in national and international conferences and received more than 245 Impact Factor. He has supervised three Ph.D. (CS) and more than 50 M.S. (CS) theses to date.

**MUHAMMAD ALMAS ANJUM** is currently a Professor with the College of Electrical & Mechanical Engineering, National University of Sciences & Technology (NUST), Pakistan. His area of specialization is pattern recognition, security systems (biometrics), and computer vision. Apart of his more than 50 international publications in his area of specialization, he is the author of a book titled *Face Recognition a Challenge in Biometrics: Image Resolution Issues in Face Recognition*. He has evaluated more than ten Ph.D. thesis. He is a reviewer/member of more than dozen international technical committees. He is also an Executive Editor of the *UW Journal of Computer Sciences*. He has completed different projects around the globe. He has been a Team lead in establishing Center of Excellence Information Technology, College of Electrical & Mechanical Engineering, and has served as its first pioneer head. He also designed and established a Center of Innovation and Entrepreneurship, College of Electrical & Mechanical Engineering. He has also served as the Dean for the Faculty of Computer Sciences, University of Wah, and the Director of Research and Development for the College of Electrical & Mechanical Engineering, NUST.

**HABIB ULLAH KHAN** (Member, IEEE) received the Ph.D. degree in management information systems from Leeds Becket University, U.K. He is currently an Associate Professor of the MIS, Department of Accounting & Information Systems, College of Business and Economics, Qatar University, Qatar. He has more than 19 years of industry, teaching, and research experience. He is an Active Researcher and his research work published in leading journals of the MIS field. His research interests include IT security, online behaviour, IT adoption in supply chain management, the Internet addiction, mobile commerce, computer mediated communication, IT outsourcing, big data, cloud computing, and E-learning. He is also a member of leading professional organizations, such as IEEE, DSI, SWDSI, ABIS, FBD, and EFMD. He is a reviewer of leading journals of his field and also working as an editor for some journals.

**MUHAMMAD SHERAZ ARSHAD MALIK** received the Ph.D. degree from University Teknoiogi PETRONAS, Malaysia. He has industrial, research, and academia experience of more than ten years in a various country at various research and senior administration roles. He is currently working as an Assistant Professor with the Department of Information Technology, Government College University Faisalabad, Pakistan, and the Chairman of the Department of Estate Care, Government College University Faisalabad. His research interests include machine learning and human interaction, data visualization, big data, digital image processing, and artificial intelligence.

**SEIFEDINE KADRY** (Senior Member, IEEE) received the bachelor's degree in applied mathematics from Lebanese University, in 1999, the M.S. degree in computation from Reims University, France, and EPFL, Lausanne, in 2002, the Ph.D. degree from Blaise Pascal University, France, in 2007, and the HDR degree in engineering science from Rouen University, in 2017. He is currently working as an Associate Professor with Beirut Arab University, Lebanon. His current research interests include education using technology, smart cities, system prognostics, stochastic systems, and probability and reliability analysis. He is also a Fellow of IET, ACSIT, and ABET Program Evaluator. He is also an Associate Editor of IEEE ACCESS journal.